


Taylor dispersion of elongated rods at small and large rotational Péclet numbers

Aditya S. Khair *

Department of Chemical Engineering, Carnegie Mellon University, Pittsburgh, Pennsylvania 15213, USA



(Received 14 September 2021; accepted 12 January 2022; published 27 January 2022)

Recently, Kumar *et al.* analyzed the Taylor dispersion of prolate spheroidal particles in a steady two-dimensional Poiseuille flow between parallel rigid walls [A. H. Kumar *et al.*, Taylor dispersion of elongated rods, *Phys. Rev. Fluids* **6**, 094501 (2021)]. They showed that the dispersivity of a spheroid is enhanced relative to that of an equivalent sphere whose translational diffusivity is equal to the orientation-averaged translational diffusivity of the spheroid. The largest enhancement in dispersivity occurs for elongated spheroids at large rotational Péclet numbers. The main purpose of this paper is to derive asymptotic approximations of the dispersivity and mean particle advection speed in these limits. Asymptotic approximations of these quantities at small rotational Péclet numbers are also presented.

DOI: [10.1103/PhysRevFluids.7.014502](https://doi.org/10.1103/PhysRevFluids.7.014502)

I. INTRODUCTION

Recently, Kumar *et al.* [1] studied the transport of Brownian prolate spheroids in two-dimensional steady Poiseuille flow between parallel rigid walls. They assumed that particle-particle and particle-wall hydrodynamic interactions were negligible; the particles translate with the local velocity of the ambient flow and orient due to the local vorticity and strain. They showed, via Monte Carlo simulations and theoretical calculations, that the particles undergo enhanced diffusion in the flow direction, i.e., Taylor dispersion. They compared the dispersion coefficient for a spheroid κ against that of an “equivalent sphere” κ_s , which refers to a spherical particle whose translational diffusivity is equal to the orientation-averaged translational diffusivity of the spheroid. Note that our choice of symbols to represent various quantities will mirror [1]. The ratio κ/κ_s is a function of the rotational Péclet number $\text{Pe}_r = U^*/a^*D_\theta^*$, where U^* is the maximum speed of the Poiseuille flow, $2a^*$ is the distance between the walls, and D_θ^* is the rotational diffusion coefficient of the spheroids. Above and henceforth, dimensional variables will carry an asterisk superscript; dimensionless variables will have no such superscript. Rotational diffusion dominates at small Pe_r ; the spheroids have an equal probability of attaining any orientation in the flow. Consequently, $\kappa/\kappa_s = 1$ at $\text{Pe}_r = 0$. The particles are biased to orient with their major axis along the flow direction as Pe_r is increased. This is accompanied by a hinderance in the diffusion of particles across the flow streamlines, since the transverse diffusivity D_\perp^* of a spheroid is smaller than the longitudinal diffusivity D_\parallel^* . Consequently, the ratio κ/κ_s grows with increasing Pe_r . The greatest enhancement in dispersion coefficient is for an elongated, or slender, spheroid, due to it having the largest disparity between transverse and longitudinal diffusivities: $D_\parallel^*/D_\perp^* \rightarrow 2$ as the particle aspect ratio $p \rightarrow \infty$. [Expressions for D_\parallel^* and D_\perp^* as functions of p are given in Eqs. (6) and (7) of [1].] It was also shown that the mean advection speed u_m^* of a spheroid is lower than the mean speed of the Poiseuille flow. These two quantities are equal for a sphere, by contrast. In the main text of [1], simulations and calculations were conducted

*akhair@andrew.cmu.edu

for particles constrained to rotate in the plane of Poiseuille flow. However, Appendix B of that paper presents calculations for unconstrained rotation, which exhibit very similar trends for κ and u_m^* as functions of Pe_r . The main contribution of the present work is to derive asymptotic approximations to κ and u_m^* for elongated particles constrained to rotate in the flow plane at large Pe_r , this being the regime where the effect of particle anisotropy on dispersion is most prominent. Asymptotic approximations of these quantities at small Pe_r are also derived.

We start with the macrotransport equation derived in [1],

$$\frac{\partial \mathcal{C}_m^*}{\partial t} + \text{Pe} u_m \frac{\partial \mathcal{C}_m^*}{\partial x} = \kappa \text{Pe}^2 \frac{\partial^2 \mathcal{C}_m^*}{\partial x^2}, \quad (1)$$

governing the evolution of the laterally averaged particle concentration \mathcal{C}_m^* . In (1), t is a dimensionless time normalized on a^{2*}/\bar{D}^* , where $\bar{D}^* = (D_{\parallel}^* + D_{\perp}^*)/2$ is the orientation-averaged translational diffusion coefficient for a spheroid constrained to rotate in the flow plane, x is a dimensionless streamwise coordinate normalized on a^* , u_m is a dimensionless mean advection speed normalized on U^* , and κPe^2 is a dimensionless dispersivity normalized on \bar{D}^* , where $\text{Pe} = U^* a^*/\bar{D}^*$ is a translational Péclet number and κ is the dispersion coefficient. The macrotransport equation is valid for times greater than a^{2*}/\bar{D}^* , when the spheroids have sampled all streamlines of the Poiseuille flow. Further, it is required that $\text{Pe}_r/\text{Pe} \ll 1$, which stipulates that a particle samples all orientations at a given streamline before it diffuses to the next streamline. The long-time solution to (1) is a Gaussian distribution with centroid moving at speed u_m and variance proportional to $\kappa \text{Pe}^2 t$. For a sphere $u_m = \frac{2}{3}$ and $\kappa = \frac{8}{945}$.

The mean particle advection speed

$$u_m = \frac{\overline{D_y^{-1} u(y)}}{D_y^{-1}} + O(\text{Pe}^{-1}). \quad (2)$$

The error of $O(\text{Pe}^{-1})$ is viewed as negligible since the results presented in [1] are for $\text{Pe} = 100$ and larger. In (2), the overline indicates a lateral average, $\overline{(\cdot)} = \frac{1}{2} \int_{-1}^1 (\cdot) dy$, where y is a dimensionless lateral coordinate (normalized on a^*), such that the top and bottom walls are at $y = 1$ and $y = -1$, respectively. The dimensionless Poiseuille flow velocity, normalized on U^* , is $u(y) = 1 - y^2$. The dimensionless orientation-averaged diffusivity $D_y(y)$ is normalized on \bar{D}^* . This quantity is defined as $D_y(y) = \langle D_{yy} g \rangle$, where D_{yy} (again, normalized on \bar{D}^*) is the yy component of the particle diffusivity tensor in the laboratory (xy) frame. This component can be written in terms of the transverse and longitudinal diffusivities as

$$D_{yy} = D_{\parallel} \sin^2 \theta + D_{\perp} \cos^2 \theta, \quad (3)$$

where θ is the counterclockwise angle from the flow direction and D_{\parallel} and D_{\perp} are normalized on \bar{D}^* . The function $g(\theta; y)$ represents the orientation distribution at each lateral position of the flow, which satisfies the boundary value problem

$$\frac{\partial^2 g}{\partial \theta^2} - \text{Pe}_r \frac{\partial}{\partial \theta} [\omega(y, \theta) g] = 0, \quad \langle g \rangle \equiv 2 \int_0^{\pi} g d\theta = 1, \quad (4)$$

where the dimensionless angular velocity for elongated particles is $\omega(y, \theta) = \dot{\gamma}(y) \sin^2 \theta$, with $\dot{\gamma}(y) = 2y$ the dimensionless shear rate of the Poiseuille flow. Both ω and $\dot{\gamma}$ are normalized on U^*/a^* . The invariance of the differential equation for g under the transformation $\theta \rightarrow \theta + \pi$ allows one to restrict the range of θ to between 0 and π . The angular brackets in the definition of $D_y(y)$ denote an integral over θ , per (4). Finally, the dispersion coefficient

$$\kappa = \frac{\overline{D_y^{-1} G(u - u_m)}}{D_y^{-1}}, \quad (5)$$

in which $G(y)$ is the iterated integral

$$G(y) = \int_{-1}^y \left[\int_{-1}^{y'} D_y^{-1}(y'') [u(y'') - u_m] dy'' \right] dy'. \quad (6)$$

II. ORIENTATION DISTRIBUTION

To proceed, we first construct an asymptotic solution to (4) at large Pe_r . Note that, after rescaling Eq. (34a) in [1] with the slow space variable $\xi = \epsilon^2 X = \epsilon^2(x - u_m t)$ and slow time variable $T = \epsilon^2 t$ defined in [1], Eq. (4) for g is recovered at leading order in $\epsilon \equiv \text{Pe}_r/\text{Pe} \ll 1$ provided $\epsilon \ll 1$ and $\text{Pe}_r \epsilon^2 \ll 1$. Thus, considering the limit $\text{Pe}_r \rightarrow \infty$ is valid provided $\text{Pe}_r \epsilon^2 \ll 1$. Numerical solutions [see Fig. 7(b) of [1]] indicate a boundary layer structure at $\text{Pe}_r \gg 1$, which can be analyzed using the approach of Brenner [2], who considered (4) for a spatially uniform shear rate, i.e., $\dot{\gamma}$ is independent of y . There exist boundary layers at $\theta = 0$ and π . We first consider the boundary layer at $\theta = 0$.

The first integral of (4) yields

$$-\frac{\partial g}{\partial \theta} + \text{Pe}_r \dot{\gamma} \sin^2 \theta g = C(y), \quad (7)$$

where $C(y)$ inherits its y dependence through $\dot{\gamma}(y)$. Balancing the second term on the left-hand side with the right-hand side gives the leading-order outer approximation $g \sim C/(\text{Pe}_r \dot{\gamma} \sin^2 \theta)$. However, this approximation breaks down as $\theta \rightarrow 0$, since $g \sim C/(\text{Pe}_r \dot{\gamma} \theta^2)$ and thus $\partial g/\partial \theta \sim -2C/(\text{Pe}_r \dot{\gamma} \theta^3)$. That is, when $\text{Pe}_r \theta^3 = O(1)$ there is a boundary layer in which we can no longer neglect the first term on the left-hand side of (7) (i.e., the effect of rotational diffusion). Thus, we define an inner coordinate $\bar{\theta} = \text{Pe}_r^{1/3} \theta = O(1)$ as $\text{Pe}_r \rightarrow \infty$ and denote g by \bar{g} in this boundary layer.

We assume (to be justified *a posteriori*) that g is asymptotically small in the outer region, so the integral in the normalization condition in (4) must have its leading-order contribution from the boundary layers. Since the boundary layer is $O(\text{Pe}_r^{-1/3})$ wide this means that $\bar{g} = O(\text{Pe}^{1/3})$ in the boundary layer to leading order; the elongated particles are mostly aligned with the strong flow. Furthermore, since $g \sim C/(\text{Pe}_r \dot{\gamma} \theta^2)$ as $\theta \rightarrow 0$ we have $C \sim \text{Pe}^{1/3} \bar{g} = O(\text{Pe}^{2/3})$ to leading order. This shows that $g = O(\text{Pe}^{-1/3})$ in the outer region, which is asymptotically small, as assumed. Thus, we define $C = \text{Pe}^{2/3} \bar{C}$, where $\bar{C} = O(1)$. To proceed, let $\bar{g} = \text{Pe}^{1/3} \bar{C} \bar{G}$ and approximate $\sin^2 \theta \sim \theta^2$ in the boundary layer, which from (7) yields

$$\frac{\partial \bar{G}}{\partial \bar{\theta}} - \dot{\gamma} \bar{\theta}^2 \bar{G} = -1. \quad (8)$$

The solution to (8) is

$$\bar{G} = 3^{-2/3} \dot{\gamma}^{-1/3} e^{(1/3)\dot{\gamma}\bar{\theta}^3} \Gamma\left(\frac{1}{3}, \frac{1}{3}\dot{\gamma}\bar{\theta}^3\right), \quad (9)$$

where $\Gamma(s, x) = \int_x^\infty t^{s-1} e^{-t} dt$ is the incomplete Gamma function. The analysis of the boundary layer at $\theta = \pi$ is almost identical: here we introduce the inner coordinate $\hat{\theta} = \text{Pe}^{1/3}(\theta - \pi)$, which is $O(1)$ as $\text{Pe}_r \rightarrow \infty$. Note that $\hat{\theta}$ is a negative quantity. We denote g by \hat{g} in this boundary layer and let $\hat{g} = \text{Pe}^{1/3} \bar{C} \hat{G}$. It is readily shown that \hat{G} is given by (9) with $\bar{\theta}$ replaced by $\hat{\theta}$. Thus, the normalization condition reduces to

$$\int_0^\infty \bar{g} d\bar{\theta} + \int_{-\infty}^0 \hat{g} d\hat{\theta} \sim \text{Pe}_r^{1/3}, \quad (10)$$

which upon substituting in \bar{g} and \hat{g} yields

$$\bar{C} = \frac{1}{2} \left[\int_{-\infty}^\infty \bar{G} d\bar{\theta} \right]^{-1} = \frac{3^{1/3}}{2[\Gamma(\frac{1}{3})]^2} \dot{\gamma}^{2/3}, \quad (11)$$

where $\Gamma(s) = \int_0^\infty t^{s-1} e^{-t} dt$ is the Gamma function. In deriving this result we have used $3^{-2/3} \int_{-\infty}^\infty e^{(1/3)y^3} \Gamma(\frac{1}{3}, \frac{t^3}{3}) dt = 3^{-1/3} [\Gamma(\frac{1}{3})]^2$ [2]. Thus, we arrive at the leading-order solution in the boundary layer at $\theta = 0$,

$$\bar{g} \sim \frac{3^{-1/3}}{2[\Gamma(\frac{1}{3})]^2} \dot{\gamma}^{1/3} e^{(1/3)\dot{\gamma}\bar{\theta}^3} \Gamma(\frac{1}{3}, \frac{1}{3}\dot{\gamma}\bar{\theta}^3) \text{Pe}_r^{1/3}, \quad (12)$$

and the leading-order solution in the boundary layer at $\theta = \pi$, namely, \hat{g} , is given by (12) with $\bar{\theta}$ replaced by $\hat{\theta}$. The leading-order outer solution is

$$g \sim \frac{3^{1/3}}{2[\Gamma(\frac{1}{3})]^2} \frac{1}{\dot{\gamma}^{1/3} \sin^2 \theta} \text{Pe}_r^{-1/3}. \quad (13)$$

The next terms in (12) and (13) are $O(\text{Pe}_r^{-1/3})$ and $O(\text{Pe}_r^{-4/3})$, respectively. As expected, Eq. (12) implies that particles are mostly aligned with the strong flow, with a small $O(\text{Pe}_r^{-1/3})$ misalignment (13). However, this analysis is not valid across the entire gap between the walls: there is a small region, $y = O(\text{Pe}_r^{-1})$, near the center where the expansion breaks down. Physically, this occurs as the vorticity of the flow is small near the center, so there is no tendency for the rods to be strongly aligned there. This effect is seen in Fig. 7(a) of [1].

III. ORIENTATION-AVERAGED DIFFUSIVITY

Next we compute the orientation-averaged diffusivity

$$D_y(y) = \langle D_{yy} g \rangle = 2 \int_0^\pi D_{yy}(\theta) g(\theta, y) d\theta. \quad (14)$$

The integral (14) is evaluated using a divide and conquer technique [3], that is, we partition it as

$$D_y(y) = \int_0^\delta D_{yy}(\theta) g(\theta, y) d\theta + \int_\delta^{\pi-\delta} D_{yy}(\theta) g(\theta, y) d\theta + \int_{\pi-\delta}^\pi D_{yy}(\theta) g(\theta, y) d\theta, \quad (15)$$

where $\text{Pe}_r^{-1/3} \ll \delta \ll 1$. Let the first integral in (15) be denoted by I_1 . Therein, g can be represented by the boundary layer solution \bar{g} [Eq. (12)], which leads to

$$\begin{aligned} I_1 &= \text{Pe}_r^{-1/3} \int_0^{\text{Pe}_r^{1/3}\delta} D_{yy}(\bar{\theta}) \bar{g}(\bar{\theta}, y) d\bar{\theta} \\ &= \frac{\dot{\gamma}^{1/3} 3^{-1/3} D_\perp}{[\Gamma(\frac{1}{3})]^2} \left[\int_0^\infty e^{(1/3)\dot{\gamma}\bar{\theta}^3} \Gamma\left(\frac{1}{3}, \frac{1}{3}\dot{\gamma}\bar{\theta}^3\right) d\bar{\theta} - \frac{3^{2/3}}{\dot{\gamma}^{2/3}} \text{Pe}_r^{-1/3} \delta^{-1} + o(\text{Pe}_r^{-1/3} \delta^{-1}) \right]. \end{aligned} \quad (16)$$

Let the third integral in (15) be denoted by I_3 . Here g is represented by the boundary layer solution \hat{g} , which yields

$$\begin{aligned} I_3 &= \text{Pe}_r^{-1/3} \int_{-\text{Pe}_r^{1/3}\delta}^0 D_{yy}(\hat{\theta}) \hat{g}(\hat{\theta}, y) d\hat{\theta} \\ &= \frac{\dot{\gamma}^{1/3} 3^{-1/3} D_\perp}{[\Gamma(\frac{1}{3})]^2} \left[\int_{-\infty}^0 e^{(1/3)\dot{\gamma}\hat{\theta}^3} \Gamma\left(\frac{1}{3}, \frac{1}{3}\dot{\gamma}\hat{\theta}^3\right) d\hat{\theta} - \frac{3^{2/3}}{\dot{\gamma}^{2/3}} \text{Pe}_r^{-1/3} \delta^{-1} + o(\text{Pe}_r^{-1/3} \delta^{-1}) \right]. \end{aligned} \quad (17)$$

Let the second integral in (15) be denoted by I_2 . Therein, g can be represented by the outer solution (13), which leads to

$$I_2 = \int_\delta^{\pi-\delta} D_{yy}(\theta) g(\theta, y) d\theta = \frac{3^{1/3} 2 D_\perp}{[\Gamma(\frac{1}{3})]^2 \dot{\gamma}^{1/3}} \text{Pe}_r^{-1/3} \delta^{-1} + \frac{3^{1/3} \pi}{[\Gamma(\frac{1}{3})]^2} \frac{D_\parallel - D_\perp}{\dot{\gamma}^{1/3}} \text{Pe}_r^{-1/3} + o(\text{Pe}_r^{-1/3}). \quad (18)$$

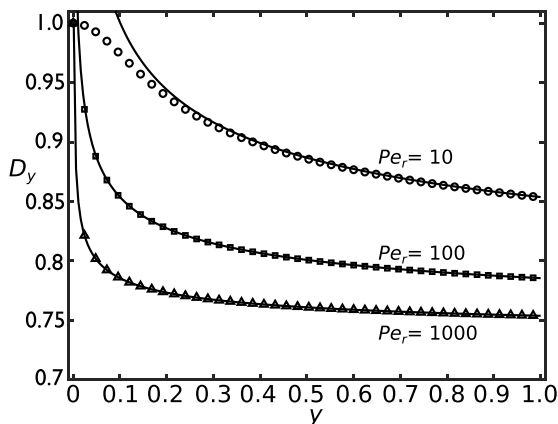


FIG. 1. Comparison of asymptotic predictions [lines, from (19)] against numerical calculations (symbols, from [1]) for the orientation-averaged diffusivity D_y at different Pe_r and $p = 1000$. The phrase “numerical calculations” pertains to numerical results from the theoretical analysis in Sec. III of [1], as opposed to the Monte Carlo simulation results therein.

Substituting (16)–(18) into (15) yields

$$D_y(y) = D_\perp \left[1 + \frac{3^{1/3}\pi}{2^{1/3}[\Gamma(\frac{1}{3})]^2} \left(\frac{D_\parallel - D_\perp}{D_\perp} \right) y^{-1/3} Pe_r^{-1/3} + o(Pe_r^{-1/3}) \right], \quad (19)$$

where we have used $\dot{\gamma} = 2y$. Equation (19) applies for $y > 0$: The symmetry of flow about $y = 0$ dictates that D_y is an even function of y ; hence, the term $y^{-1/3}$ is replaced by $|y|^{-1/3}$ for $y < 0$. Note that (19) loses uniformity at $|y| = O(Pe_r^{-1})$. The error in (19) is expected to be $O(Pe_r^{-2/3})$, which arises from the second, $O(Pe_r^{-1/3})$, term in the boundary layer expansions. A comparison of (19) with the numerical calculations of [1] is given in Fig. 1.

IV. DISPERSION COEFFICIENT AND MEAN PARTICLE ADVECTION SPEED

Using (19) we evaluate the mean advection speed u_m [Eq. (2)] and dispersion coefficient κ [Eq. (5)]. These quantities involve integrals over the entire y domain, but (19) is invalid for $|y| = O(Pe_r^{-1})$. However, the contributions to these integrals from this near-center region are at most $O(Pe_r^{-1})$ and therefore subdominant to the expressions we present below.

Inserting (19) into (2) yields

$$u_m = \frac{2}{3} - \frac{3^{1/3}\pi}{2^{10/3}[\Gamma(\frac{1}{3})]^2} \left(\frac{D_\parallel - D_\perp}{D_\perp} \right) Pe_r^{-1/3} + O(Pe_r^{-2/3}). \quad (20)$$

Inserting (19) into (6) yields

$$\begin{aligned} G(y) = & \frac{1}{D_\perp} \left[-\frac{1}{12}(y^2 - 1)^2 \right. \\ & + \frac{1}{880} \frac{3^{1/3}\pi}{2^{1/3}[\Gamma(\frac{1}{3})]^2} \left(\frac{D_\parallel - D_\perp}{D_\perp} \right) (119 - 264|y|^{5/3} + 55y^2 + 90|y|^{11/3}) Pe_r^{-1/3} \left. \right] \\ & + O(Pe_r^{-2/3}). \end{aligned} \quad (21)$$

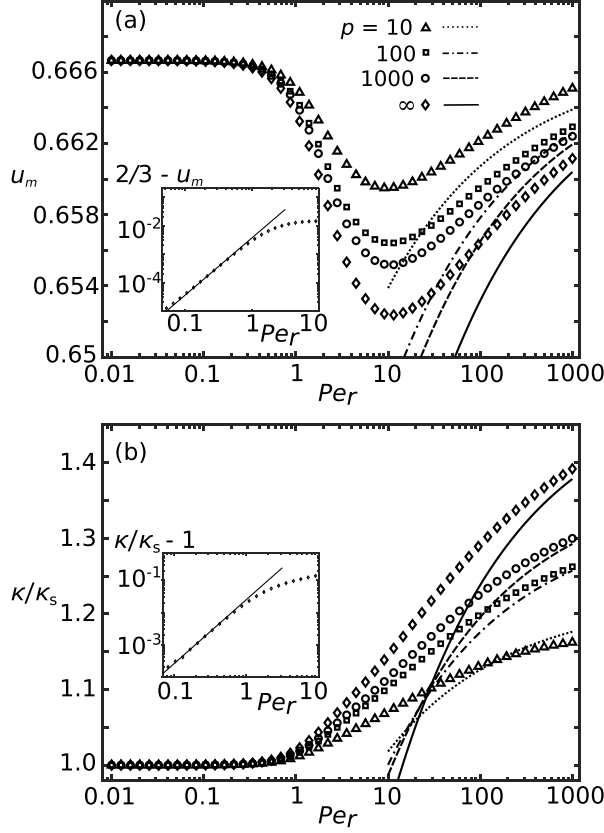


FIG. 2. Comparison of asymptotic predictions at large Pe_r [lines, from (20) and (22)] against numerical calculations (symbols, from [1]) for (a) mean advection speed u_m and (b) dispersion coefficient κ/κ_s . Here $Pe = 1000$ and again the numerical calculations pertain to numerical results from the theoretical analysis in Sec. III of [1], as opposed to the Monte Carlo simulation results therein. The inset in (a) plots $\frac{2}{3} - u_m$ versus Pe_r for $p \rightarrow \infty$, which shows agreement between the small- Pe_r expansion (23) and the numerical calculations. The inset in (b) plots $\kappa/\kappa_s - 1$ versus Pe_r for $p \rightarrow \infty$, which shows agreement between the small- Pe_r expansion (24) and the numerical calculations.

Using (21) with (5) returns

$$\kappa = \frac{1}{D_{\perp}} \left[\frac{8}{945} - \frac{23}{1680} \frac{3^{1/3} \pi}{2^{1/3} [\Gamma(\frac{1}{3})]^2} \left(\frac{D_{\parallel} - D_{\perp}}{D_{\perp}} \right) Pe_r^{-1/3} + O(Pe_r^{-2/3}) \right]. \quad (22)$$

A comparison of (20) and (22) with the numerical calculations of [1] is given in Fig. 2. The agreement between the asymptotics and numerics is consistent with the error in (20) and (22) being $O(Pe_r^{-2/3})$. Thus, better agreement would be observed at larger Pe_r than shown in Fig. 2; the results in [1] were up to $Pe_r = 1000$. At $Pe_r > 1000$ it may not be necessary to increase Pe such that $\epsilon \ll 1$ since in Fig. 9 of [1] good agreement is seen between the Monte Carlo simulations and theoretical calculations at $Pe_r = 1000$ and $Pe = 1000$, for which $\epsilon = 1$.

V. CONCLUSION

The primary results of this paper are the asymptotic expressions for the mean particle advection speed (20) and dispersion coefficient (22) at large Pe_r . These expressions can be further simplified

in the limit of a very slender particle by noting that $D_{\parallel}/D_{\perp} \rightarrow 2$ and $D_{\perp} \rightarrow \frac{2}{3}$ as $p \rightarrow \infty$. A companion analysis at small Pe_r is straightforward since the limit $\text{Pe}_r \rightarrow 0$ is regular. The details are presented in the Appendix; the asymptotic series for u_m and κ through $O(\text{Pe}_r^2)$ are

$$u_m = \frac{2}{3} - \frac{1}{90} \left(\frac{D_{\parallel} - D_{\perp}}{D_{\parallel} + D_{\perp}} \right) \text{Pe}_r^2 + O(\text{Pe}_r^3) \quad (23)$$

and

$$\kappa = \left(\frac{2}{D_{\parallel} + D_{\perp}} \right) \left(\frac{8}{945} \right) \left[1 + \frac{3}{40} \left(\frac{D_{\parallel} - D_{\perp}}{D_{\parallel} + D_{\perp}} \right) \text{Pe}_r^2 + O(\text{Pe}_r^3) \right], \quad (24)$$

which compare favorably to [1] (see the insets in Fig. 2).

It would be interesting to consider other types of unidirectional flow, such as electro-osmotic flow, pressure-driven flow between walls with hydrodynamic slip, or a combination of Couette flow and pressure-driven flow. In fact, much of the present analysis remains valid: The orientation-averaged diffusivity is still given by (19) (with y replaced by $\dot{\gamma}/2$). However, the increased algebraic complexity of the shear rate in these flows means that the integrals for u_m and κ would likely have to be performed numerically. Nonetheless, the large- Pe_r expansions of u_m and κ remain of the form given in (20) and (22), respectively, although the coefficient of the $O(\text{Pe}_r^{-1/3})$ contribution will depend on flow type. Finally, an analysis of the unconstrained rotation problem at large Pe_r would be desirable. This is of course more challenging as the orientation distribution now satisfies a partial differential equation. It is therefore fortunate that the numerical results in [1] for unconstrained rotation are so similar to the constrained problem. Thus, our analysis should be of practical utility.

ACKNOWLEDGMENTS

I thank Daniel Harris and Ajay Harishankar Kumar for supplying data from [1].

APPENDIX: SMALL- Pe_r ANALYSIS

At $\text{Pe}_r \ll 1$ we pose the regular expansions $g = g_0 + g_1 \text{Pe}_r + g_2 \text{Pe}_r^2 + O(\text{Pe}_r^3)$ and $C = C_1 \text{Pe}_r + C_2 \text{Pe}_r^2 + O(\text{Pe}_r^3)$. Inserting said expansions into (7) yields

$$g_0 = \frac{1}{2\pi}, \quad (A1)$$

$$g_1 = -\frac{\dot{\gamma}}{8\pi} \sin(2\theta), \quad (A2)$$

$$g_2 = \frac{\dot{\gamma}^2}{128\pi} [4 \cos(2\theta) - \cos(4\theta)], \quad (A3)$$

along with $C_1 = \dot{\gamma}/4\pi$ and $C_2 = 0$. Using (A1)–(A3) with (14) gives

$$D_y(y) = \frac{D_{\parallel} + D_{\perp}}{2} - \left(\frac{D_{\parallel} - D_{\perp}}{16} \right) y^2 \text{Pe}_r^2 + O(\text{Pe}_r^3). \quad (A4)$$

Inserting (A4) into (2) and (5) yields (23) and (24), respectively.

-
- [1] A. H. Kumar, S. J. Thomson, T. R. Powers, and D. M. Harris, Taylor dispersion of elongated rods, *Phys. Rev. Fluids* **6**, 094501 (2021).
[2] H. Brenner, Orientation-space boundary layers in problems of rotational diffusion and convection at large rotary Péclet numbers, *J. Colloid Interface Sci.* **34**, 103 (1970).
[3] E. J. Hinch, *Perturbation Methods* (Cambridge University Press, Cambridge, 1991).